Journal of Materials Chemistry A

NanoMOFs: Little crystallites for substantial applications

Journal:	*Journal of Materials Chemistry A*
Manuscript ID	TA-REV-03-2018-002132.R1
Article Type:	Review Article
Date Submitted by the Author:	05-Apr-2018
Complete List of Authors:	Majewski, Marek; Concordia University, Chemistry and Biochemistry Noh, Hyunho; Northwestern University Islamoglu, Timur; Northwestern University, Department of Chemistry Farha, Omar; Northwestern University, Chemistry

Journal Name

ARTICLE

NanoMOFs: Little crystallites for substantial applications

M. B. Majewski,[a] H. Noh,[b] T. Islamoglu,[b] O. K. Farha[b,c]

Received 00th January 20xx,
Accepted 00th January 20xx

DOI: 10.1039/x0xx00000x

www.rsc.org/

In order to tailor metal–organic framework (MOF) materials for a myriad of potential applications, recent studies have expanded on the advantages of using MOF particles in the nano-size regime. These so-called nanoMOFs may be prepared using a variety of synthetic methodologies; many analogous to those used for the preparation of their bulk counterparts. However, many of these techniques lack the refinement to consistently produce monodisperse particle sizes. Here we discuss recent advances in some of these synthetic methods with a particular emphasis on methods exhibiting increased levels of size-control while producing crystallites ranging in size from 10s to 100s of nanometers. Additionally, we highlight some specific appplications that benefit from the inherent properties of nano-sized MOFs.

1. Introduction

Nano-sized crystals, typically with dimensions in the range 5-500 nm,[1, 2] can offer unique opportunities for enhancing the physical and/or chemical properties of their bulk counterparts,[3-5] or for generating novel properties for new applications.[6, 7] Classically, photo/electroluminescent or surface properties of nanocrystals have been examined for potential applications as chromophores[3-5, 8, 9] or as heterogeneous catalysts.[6, 7, 10, 11] In the former case, confinement effects based on crystal size (in the nano-regime) engender unique optical properties in the crystals; effects which can be fine-tuned by adjusting their size and morphology.[12-14] In heterogeneous catalysis, nano-sizing the crystalline catalysts can 1) present a higher density of catalytic sites on the surface due to significant increase in specific surface area and 2) allow faster and more facile substrate-catalyst interaction due to lower diffusion barriers and/or shorter *in-crystal* diffusion distances.[15-20] Consequently, nano-sized catalysts commonly outperform in their catalytic (kinetic) rates as compared to their equimolar bulk analogues. More recently, morphological control, or increasing the external area of desired crystal facets for catalysis, has been examined *via* addition of well-faceted seeds or various surfactants.[18-20] Beyond the aforementioned applications, porous nanocrystals such as zeolites have been applied to chemical sensing,[21-23] bio-imaging and drug delivery.[24-26] In biological applications, nano-zeolites serve as effective encapsulants (trapping target molecules within the pores), that rapidly diffuse through capillary vessels or lymphatic systems given their dimensions, and subsequently release encapsulated molecules at desired sites.

With large cavities presented in a periodic fashion—leading to high internal surface area—metal–organic frameworks (MOFs) constitute one of the most widely studied porous crystalline materials.[27-30] Through careful design of both the inorganic node and the organic linker, the confined physical and chemical environment within the pores of a MOF can be rationally manipulated to create materials with unique properties.[31-38] Further modulation of the framework can be achieved *via* post-synthetic modifications where metal complexes,[39-43] metal chalcogenide clusters,[44-53] organic functional groups,[54-59] or enzymes[36, 37, 60-63] can be encapsulated, covalently bound, or associated with the framework. Given this versatility, MOFs have been exploited for a wide range of applications including gas storage,[28, 32, 36, 38, 64-67] gaseous/condensed phase separation,[55, 56, 68-75] light harvesting,[76-80] chemical sensing,[81-85] membranes,[86-90] biomedical,[91-93] and heterogeneous catalysis.[33, 36, 40, 41, 44-48, 51, 52, 54, 59-61, 63] While the first synthesis of network structures with large, repeating channels was presented in 1994[94] and the "MOF" moniker was coined in 1995,[95] synthesis and applications of nanoMOFs (NMOFs)—purpose-synthesized MOF nano-crystallites—were not realized until more recently.[60, 61, 96-99] NMOFs typically retain high porosity (often mesoporosity where pore size falls within the range of 2–50 nm)[60, 61] as observed in the bulk materials making these materials particularly competent for catalysis where substrates can readily diffuse to the centre of the crystals, thereby capitalizing on nearly all catalytic sites presented in the MOF pores to enhance the apparent catalytic rate.

Coupled with synthetic protocols such as hydrothermal, or microwave/ultrasound-assisted syntheses that have been traditionally reserved for other nano-sized materials, coordination modulation *via* additives (modulators) that compete for coordination with the secondary building units (SBUs) have also been proven to yield various MOF crystallites

[a] Department of Chemistry and Biochemistry, Concordia University, 7141 Sherbrooke Street West, Montreal H4B 1R6, Canada.
[b] Department of Chemistry, Northwestern University, 2145 Sheridan Road, Evanston, Illinois 60208-3113, USA.
[c] Department of Chemistry, Faculty of Science, King Abdulaziz University, Jeddah, Saudi Arabia

in the nano-regime. These crystallites are subsequently amenable to many potential applications, where herein we highlight three general categories: 1) catalysis where the MOF itself serves as the catalyst, or as a support for a post-synthetically introduced catalyst, 2) bio-imaging and drug delivery, and 3) chemical sensing. The highlights of this emerging subclass of porous materials intend to not only emphasize their advantages compared to their bulk counterparts, but also to underline how NMOFs may act as superior substitutes to other well-established nanocrystals.

Several comprehensive overviews exist covering NMOF syntheses for specific applications, along with general methods for NMOF preparation.[100-103] This review seeks to augment and update these works by highlighting some recent studies where the authors report precise control over the preparation of MOF crystallite size followed by some example applications where NMOFs are showing promise.

2. Synthetic methods for NMOF preparation

In recent years, many prevalent synthetic methods have been developed for preparing MOF materials in nano-, micro- and larger size regimes.[104] Oftentimes, these methods are analogous to one another without exercising size control. Conscious modifications to known procedures can be exploited to generate materials in the nano-regime, improving the efficiency of known applications while paving the way for new applications. In this section, the focus will be on significant recent advances in synthetic methodologies for developing nano-sized crystals of MOF materials with a focus on the differences between these methods and those used to prepare MOF materials without size control. As mentioned at the outset, general synthetic strategies for NMOF synthesis include solvothermal, microwave and sonochemical, microemulsion/reverse microemulsion, and surfactant-mediated or templated solvothermal/hydrothermal methods.

We note that a variety of experimental techniques have been evaluated for quantifying the size of NMOF crystallites formed through these various synthetic approaches.[105] Some typical experimental methods include transmission and scanning electron microscopy (TEM and SEM), atomic force microscopy (AFM), photon correlation spectroscopy (PSC), powder X-ray diffraction (PXRD) and dynamic light scattering (DLS). Most commonly, and certainly for those data highlighted in this overview, particle sizes are reported by way of PXRD and SEM measurements. We also note that X-ray diffraction methods (including those involving synchrotron radiation) along with static light scattering (SLS) and AFM have been used somewhat extensively to investigate the mechanisms of MOF formation both *ex* and *in situ*.[103]

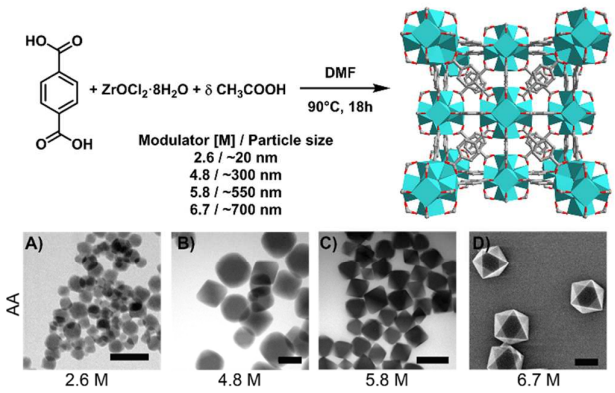

Figure 1. The effect of modulator (in this case, acetic acid) on the solvothermally synthesized crystallite size of UiO-66 as reported by Morris *et al.* Scale bar sizes; A = 100 nm, B = 200 nm, C = 500 nm, D = 500 nm. SEM micrographs reprinted with permission from Morris, W. *et al. ACS Appl. Mater. Interfaces,* 2017**, 9**, 33413-33418. Copyright 2017 American Chemical Society.

2.1 Solvothermal methodologies

Solvothermal methods have been most widely explored, and arguably remain one of the most effective methods for the preparation of MOF materials in all size regimes. One key difference in the application of solvothermal methods for NMOF synthesis is rooted in judicious selection of chemical modulator, followed closely by controlling key reaction conditions such as reaction volume, concentration, temperature (notably, NMOFs have been prepared via room temperature syntheses[106, 107]) and time.

In one representative example, Xia *et al.* synthesized Co-based ZIF-67 particles of varying sizes simply through controlling the solvothermal reaction temperature and time.[108] Bulk ZIF-67 was prepared by combining $Co(Ac)_2{\cdot}4H_2O$ with 2-methylimidazole in ethanol and heating the reaction mixture to 120°C for 3 days, while 800 nm particles were synthesized from methanol at 60°C (20 h) and corresponding 300 nm particles were also synthesized from methanol but at 25°C (20 h). Pyrolysis of the smallest particles yielded a material that acts as a competent catalyst for oxygen reduction, where catalyst derived from the smallest crystallites is superior to that derived from the larger particles (likely due to superior mass- and electron-transport properties coupled with a more completely exposed nanostructure).

Solvothermal strategies that decouple MOF nucleation and growth are appealing, as it is generally well understood that fast nucleation results in small MOF crystallites (nucleation occurs in parallel to growth). Lan *et al.* have recently reported the preparation of Zn-based ZIF-8 as well as ZnCo bimetallic NMOFs by adding a small amount of pre-formed metal node to a solution of the organic linker to generate clusters that act as seeds for follow-on crystal growth.[109] This strategy yields monodisperse ZIF-8 particles 27 nm in size (the final particle size may be modulated by varying the amount of pre-formed node added). Incorporating Pt nanoparticles into the NMOF in order to quantify internal diffusion rates highlighted the advantages of using nanoscale materials in catalysis (Section 3.1), as the highest activity for the hydrogenation of 1-hexene was observed in Pt@ZIF-8 NMOFs 45 nm in size (particle sizes of 440 nm were found to exhibit an activity that was 11-fold lower).

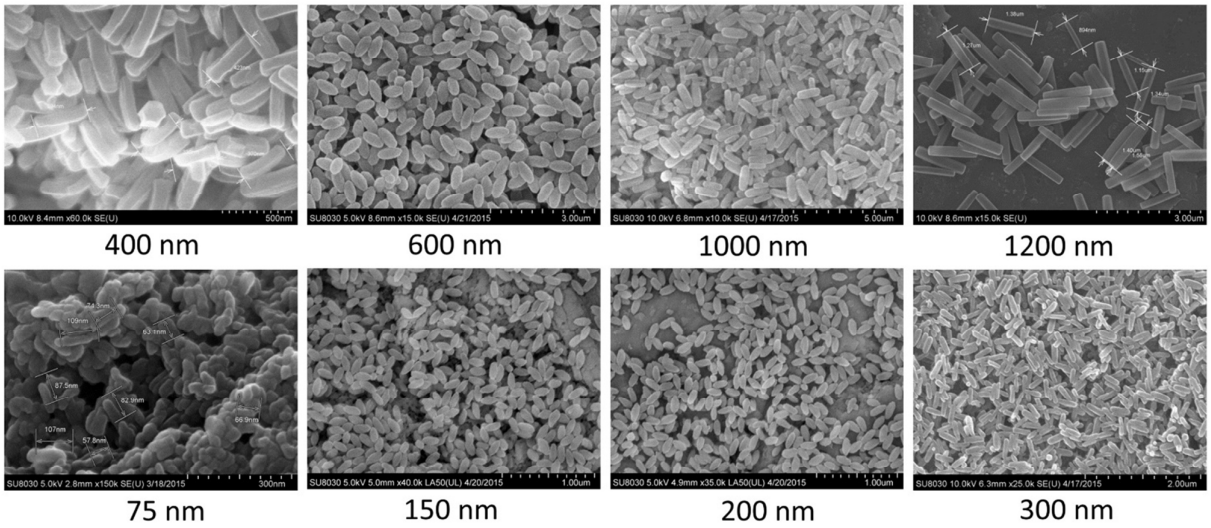

Figure 2. Scanning electron microscope (SEM) micrographs of NU-1000 MOF crystallites of varying size prepared by controlled solvothermal synthesis where two modulators are introduced at varying concentrations along with carefully selected heating temperatures and times. Unpublished results from our lab.

Introducing varying concentrations of modulators (typically monodentate competing ligands) results in different crystallite sizes through a mechanism where competition for metal binding sites takes place influencing the number of available nucleation sites.[110] In addition, introduction of modulator also leads to defects (missing linkers or metal clusters) in the final framework structure, as ligands are replaced by modulator moieties.[111] The importance of defect sites in various applications has previously been highlighted,[43, 112] and emphasizes that the solvothermal conditions employed for synthesis may control both the morphology of the bulk crystals and the sizes of the MOF crystallites.

An early example of modulated solvothermal MOF synthesis was reported by Schaate *et al.* where the preparation of Zr-based MOFs (from the UiO family) was size controlled through the influence of benzoic acid addition.[113] Adding up to three equivalents of benzoic acid was found to result in a broadening of the powder X-ray diffraction (PXRD) patterns of these materials, correlating to smaller crystal sizes (ca. 230 nm–1 μm). Small UiO-66 and UiO-67 particles can also be prepared by simply introducing HCl as a modulator, as reported by Katz *et al*.[114] Recently, and in a key follow-up study, Morris *et al.* systematically evaluated the consequences of a series of carboxylic acid modulators on MOF (specifically Zr-based UiO) formation in order to elucidate modulator effects on surface properties at the nanoscale along with colloidal stability.[115] Importantly, this work highlighted the consequences of modulator identity and concentration on the surface charge of MOF crystallites (an indicator of colloidal stability) and size dispersity (Figure 1). Varying the identity of modulator acid R-COOH (where R = H, CH_3, CF_3, and $CHCl_2$) leads to the controlled synthesis of crystallites varying in size (20 nm–1 μm), while controlling acid concentration leads to different crystallite morphologies (with low concentrations leading to quasi-spherical morphologies and higher concentrations leading to the formation of octahedral morphologies).

Hu *et al.* probed the differences in solvothermally formed morphologies of NH_2-MIL-125 (a Ti-based MOF) as a function of either small monodentate acids (acetic acid, thioglycolic acid) or "pseudolinker" acids (benzoic acid, *p*-toluylic acid).[116] In the presence of increasing concentrations of pseudolinker modulators, the crystallite size of NH_2-MIL-125 first decreased and then gradually began to increase (resulting in a "U-shaped" size versus modulator concentration profile) as the ratio of modulator-to-linker increased. In the case of *p*-toluylic acid, particle sizes decreased from ca. 800 nm (in bulk NH_2-MIL-125) to ~70–90 nm (when the modulator-to-linker ratio increased to 10), and subsequently grew to ca. 700 nm (as the ratio approached 20). Presumably this phenomenon is a direct result of modulator concentration (within a specific range) increasing nucleation rates (while also impacting the number of defect sites and pore size distribution). This same trend was not observed for the small monodentate acid modulators which (on increasing the ratio of modulator-to-linker) linearly decreased particle sizes while varying the particle morphology (in this case from circular plates to truncated octahedrons).

Extending modulator controlled synthetic methods to MOFs composed of linkers with multitopic ligands is challenging owing to the possibility of forming different nets and phases (*e.g.* a Zr_6-based MOF with a tetratopic linker can form multiple nets including but not limited to ftw and csq). Ostensibly, the formation of these phases and nets may be sensitive to the concentration of modulator (among other conditions). In an illustrative case-study of how modifications to solvothermal synthesis may be used to control NMOF crystallite size in even complicated scenarios where multitopic linkers are used, Li *et al.* found that preparing NU-1000 from $ZrOCl_2 \cdot 8H_2O$ and 1,3,6,8-tetrakis(p-benzoic acid)pyrene in the presence of two modulators enables the controlled formation of nano-sized crystallites.[60] More specifically, lowering the concentration of benzoic acid conventionally used to promote the formation of Zr_6 clusters and adding a second

monocarboxylic acid modulator, trifluoroacetic acid, results in the formation of crystallites of NU-1000 with mean sizes ranging from 75 nm up to 1.2 µm (Figure 2). Here, along with

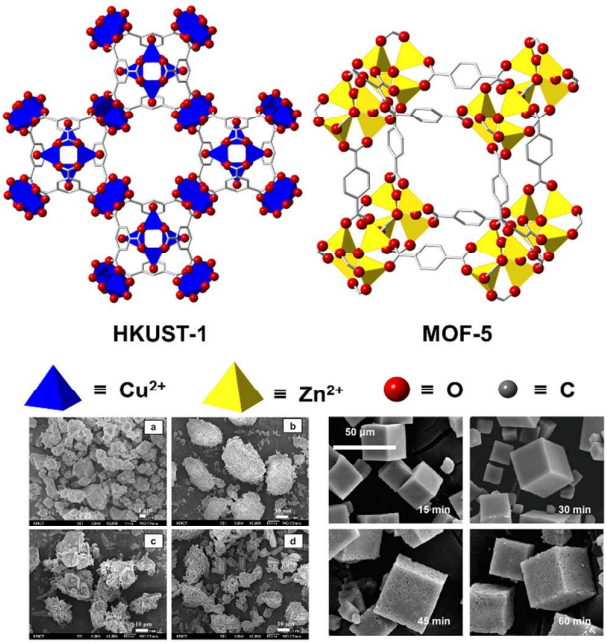

Figure 3. Structures and SEM micrographs of HKUST-1 and MOF-5 crystallites prepared by varying irradiation power, time and solvent effects during microwave synthesis. SEM micrographs reprinted with permission from Y.-K. Seo *et al. Microporous Mesoporous Mater.*, 2009, **119**, 331-337 and J.-S. Choi *et al. Microporous Mesoporous Mater.*, 2008, **116**, 727-731. Copyright 2009 and 2008 Elsevier Inc.

modulator influences, both the temperature of reaction (100–120°C) along with reaction time (0.5–1 h) play a concerted role. As expected, crystallite sizes directly correlate to the ability of this MOF to drive the hydrolysis of a nerve gas simulant (Section 3.1). An extension of this synthetic approach was used to prepare NU-1003 from 1,3,6,8-tetra(6-carboxynaphthalen-2-yl)pyrene, $ZrOCl_2 \cdot 8H_2O$, benzoic acid, and trifluoroacetic acid.[61] Crystallites ranging in size from 300 nm to 10 µm are accessed simply through adding increased equivalents of trifluoroacetic acid with identical reaction times and temperatures (3 h and 120°C, respectively). These crystallites were used to stabilize organophosphorus acid anhydrolase (OPAA) an enzyme that was then used to catalyze the degradation of another nerve agent simulant (Section 3.1).

2.2 Sonochemical and microwave approaches

In the use of solvothermal methods for MOF synthesis, it is well established that employing elevated temperatures eliminates rapid precipitation of product affording increased crystallization while solubilizing precursors. Microwave heating allows short reaction times coupled with increased kinetics of crystal nucleation through rapid energy transfer and high instantaneous temperature.[117] Thus, accelerated synthesis, phase selectivity, and most importantly, the desire for crystal size reduction has led to the adoption of microwave synthesis for the preparation of NMOF materials.[118-121]

One of the earliest examples of both modulated and microwave NMOF synthesis was reported by Diring *et al.* where HKUST-1 [$Cu_3(btc)_2$] (btc = benzene-1,3,5-tricarboxylate) was prepared in a microwave reaction (140°C, 10 min) in the presence of *n*-dodecanoic acid modulator.[110] Depending on modulator ratio (with respect to tricarboxylic acid linker), different particle morphologies and sizes were recorded. At low ratios (i.e. low concentrations of modulator) particles with sizes of ca. 20 nm formed, while increasing the ratio yielded crystallites 2 µm in size. By controlling the nucleation process in crystallite formation, addition of modulator not only afforded the ability to finely tune NMOF particle size but resulted in materials with an improved degree of crystallinity.

Recently, the role of both reaction solvent and basic modulator addition was probed in the formation of benzenetriazolate Zn-based MFU-4 in both solvothermal and microwave synthetic procedures.[105] Solvothermal synthesis of this MOF in the absence of modulator resulted in particles with sizes outside the nano-regime (ca. 1.2 µm) unless a base, lutidine, was added to the reaction mixture (resulting in particles 119 nm in size, as observed by DLS). A similar observation was made for the microwave-assisted synthesis where particle sizes of ca. 1.2 µm were observed—albeit with a much shorter reaction time; 2–10 min versus 1 day of solvothermal synthesis. However, introducing alkali hydroxides (NaOH and KOH) into the reaction resulted in crystallites ranging in size between 25–36 nm (as determined by TEM). As opposed to many of the studies mentioned in this overview, the additive here is expected to interact with the free organic linker (a weak acid) via a mechanism where the additive is responsible for linker deprotonation resulting in higher nucleation rates and smaller crystallite sizes. Conversely, adding coordination modulators triethylamine, diethylamine and *n*-hexylamine also gave rise to smaller crystallite sizes (54–188 nm as observed by TEM) as expected. This expansive study also highlighted the differences between the various techniques of NMOF size quantification where particle sizes determined by DLS and PXRD were ca. 9-17 nm larger than those observed directly via electron microscopy methods.

The multitude of variables (from irradiation power and time to solvent effects) associated with microwave synthesis of NMOFs has been thoroughly evaluated for ubiquitous MOFs such as HKUST-1 (resulting in 1–20 µm crystallites) and MOF-5 (resulting in larger 20–25 µm crystallites, Figure 3).[122, 123] UiO-66 has also been prepared by microwave methods, and Taddei *et al.* have demonstrated the scalability of this synthetic approach by employing a multi-mode apparatus that affords the irradiation of eight 30 mL reaction chambers at one time.[124]

Sonochemical synthetic methods also encourage rapid kinetics while influencing particle morphology and phase selectivity by promoting nucleation through the growth and collapse of acoustic cavitations resulting in high local temperatures (>5000 K) and pressures.[125] This is somewhat in contrast to microwave syntheses where the applied electric field results in a rapid heating of the liquid phase

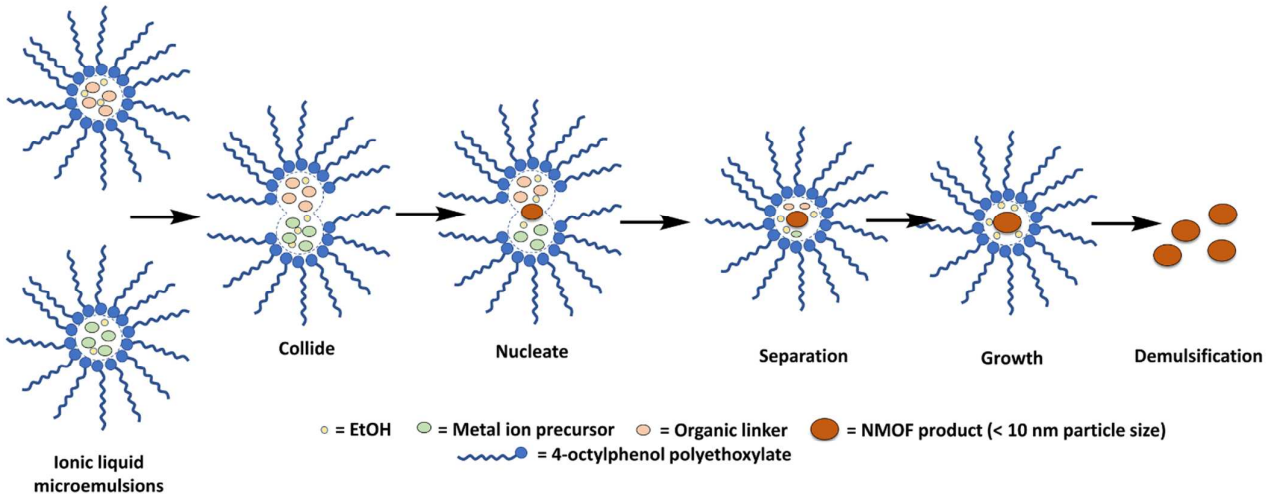

Figure 4. Schematic representation of the ionic liquid microemuslion induced growth mechanism of NMOF HKUST-1 prepared in an ionic liquid microemulsion. Adapted from ref. 138.

Much like microwave syntheses sonochemical methods have also successfully been used to prepare NMOF materials.[126-130] In an illustrative example, Li *et al*. prepared core-shell nanoparticles of HKUST-1@SiO_2 in the 200–400 nm size regime by sonochemical methods.[131] These hybrid materials are accessed by combining precursors (linkers, metal salts, and a silicate) for both components in one ultrasonic solution. In a typical reaction, HKUST-1 nanocrystals form initially, followed by growth of a SiO_2 shell resulting in a core-shell arrangement where the SiO_2 shell encompasses a single MOF core. The resulting materials were evaluated and confirmed as competent catalysts for photocatalytic phenol degradation.

2.3 Microemulsion and surfactant-mediated syntheses

Employing surfactants to control supramolecular structure has been used in template-directed synthesis of mesostructured hierarchical materials such as metal oxides and silicas.[132-134] In an early adaptation and translation of this synthetic strategy to MOF materials, Qiu and coworkers synthesized HKUST-1 around micelles formed from cetyltrimethylammonium bromide (CTAB) surfactant in EtOH/H_2O with little control over crystallite size.[135] In an elaboration of this early work, and incorporating crystallite size control, Zhao *et al*. prepared MOF nanospheres (averaging just 80 nm in diameter) by reacting a Zn salt, 1,4-benzenecarboxylic acid, ionic liquid 1,1,3,3-tetramethylguanidinium acetate, and surfactant *N*-ethyl perfluorooctylsulfonamide, in supercritical CO_2.[136] The resulting NMOF materials form through a mechanism where the surfactant molecules self-assemble into cylindrical micelles with fluorocarbon chains pointed towards a central CO_2 core surrounded by a continuous phase of the ionic liquid, Zn salt and linker. Subsequently, the metal ions, linker, and ionic liquid assemble into a microporous framework with cavities built around the micelles.

Ionic liquid microemulsions have also been used to prepare lanthanum-based NMOFs (crystallite sizes approaching 200 nm),[137] and most recently, the favorable templating properties of ionic liquids have been taken advantage of by Zheng *et al.* to prepare ZIF-8 and ZIF-67.[138] The H_2O/1-butyl-3-methylimidazolium hexafluorophosphate/4-octylphenol polyethoxylate microemulsion can be exploited to enable dissolution of the organic linkers of ZIFs (2-methylimidazole) which are water soluble. The subsequent coordination reaction takes place in (nano)water droplets (Figure 4). Adding EtOH to the microemulsion mixture enables the formation of HKUST-1, a MOF where the organic linker benzene-1,3,5-tricarboxylate is not readily soluble in water. Using this approach, mean crystallite sizes of 2.2 nm, 2.3 nm and 1.6 nm for ZIF-8, ZIF-67 and HKUST-1, respectively, are obtainable; particle sizes that are two orders of magnitude smaller than those previously reported using analogous ionic liquid microemulsion techniques. Particles this small are comprised of one or less crystallographic unit cells (assuming a lack of defect sites), a particularly intriguing observation. Indeed, 1.6 nm particles of HKUST-1 are comprised of slightly more than half of one unit cell (the unit cell of HKUST-1 measures 26.30 Å across each cubic face), while 2.2 nm and 2.3 nm particles of ZIF-8 and ZIF-67 represent just over one unit cell (where these MOFs have cubic unit cells measuring 14.74 Å and 16.96 Å respectively).

In order to generate a hierarchical composite structure using surfactant-mediated synthesis, Seoane *et al.* have shown that it is possible to prepare Al-based MIL-96, MIL-100 and MIL-110 in the presence of CTAB where varying the solvent and pH governs which MIL topology is formed (Figure 5).[139] Small crystallites of MIL-100 (ca. 30 nm) are obtained in synthetic conditions where the solvent (H_2O/EtOH) molar ratio is 3.4 (pH 2.6 in the presence of CTAB). Under these conditions, an increased concentration of EtOH reduces the size of the CTAB micelles (driving faster exchange between a hydrophilic metal ion-containing phase, and the hydrophobic linker-containing phase) while improving the solubility of the organic linker. This dynamic interaction (increased exchange kinetics) leads to the formation of smaller MIL-100 crystallites generating a

secondary mesoporosity in the resulting composite. Long-range hierarchy is created through the combination of the mesoporosity resulting from the packing of the crystallites and the microporosity inherent to the MOF.

A surfactant-mediated synthetic strategy was also used to prepare truncated rhombic dodecahedral (TRD) ZIF-8 particles (178–227 nm) in the presence of CTAB by Avci *et al*.; particles

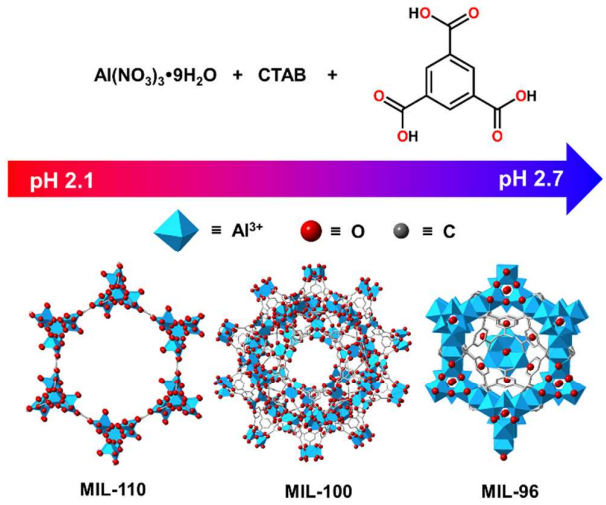

Figure 5. Varying the reaction pH during the synthesis of MIL MOFs in the presence of CTAB enables control of which MIL topology is formed. Adapted from ref. 139.

that were subsequently found to self-assemble into millimeter-size three-dimensional superstructures on evaporative drying.[140] The resulting NMOF-based superstructures exhibit angle-dependent opalescence owing to the formation of a photonic bandgap enabling the use of these materials as optical sensors for various chemical vapors.

2.4 Alternative methods

MOFs and NMOFs have also been prepared using synthetic routes that fall outside of those considered as traditional including spray-drying,[141] centrifugation,[142] hydrothermal syntheses on substrates,[90, 143] diffusion-mediated[144] and self-exfoliation techniques to yield nanosheets.[145] Of interest are synthetic methods that employ benign reaction conditions, lower energy processes, and methods that may be readily scaled upwards for eventual industrial and commercialization applications.

Preparation of a porous MOF via mechanochemistry was first reported in 2006,[146] and this synthetic methodology has since been expanded to include multicomponent reactions to prepare cocrystals, polymers and other metal-organic materials.[147] Owing to the limited predictability of mechanically breaking intramolecular bonds to instantiate a chemical reaction, few examples exist of controlled NMOF synthesis via mechanochemistry. Tröbs and Emmerling have reported the preparation of a Bi-based NMOF in a conventional ball mill, work that represents a tantalizing new synthetic approach.[148] $Bi(NO_3)_3$, benzene-1,4-dicarboxylic acid, and imidazole were ground together and the product MOF was found to form (via lab scale X-ray diffraction) after a reaction period of 2 min with a corresponding particle size of 108 nm. The reaction proceeds via a mechanism where protonation of the imidazole followed H_2O and NO_x release, resulting in an intermediate Bi species surrounded by a coordination sphere of H_2O that readily reacts with benzene-1,4-dicarboxylic acid.

While many of the preparative methods discussed herein, including mechanochemistry, can yield gram-quantities of MOF and NMOF materials, batch-to-batch and particle size reproducibility remain challenging. Droplet-based microfluidic syntheses have been previously explored to alleviate the shortcomings of some conventional MOF synthetic methods.[149-153] One noteworthy advantage of microfluidic synthesis, depending on system design, is the ability to integrate framework synthesis with post-synthetic modification and particle size control as illustrated by Jambovane *et al*. who reported the continuous preparation and post-synthetic modification of amino-modified UiO-66.[154] Combining all the components of the MOF in an oil phase to yield droplet nanoreactors which are then subjected to a residence time in a temperature controlled oven yielded NH_2-UiO-66 crystallites 80–100nm in size. Crystallite size is established through the addition of modulator as one of the reagents at the beginning of the process, in a *de facto* solvothermal synthetic arrangement, something that previous microfluidic systems have lacked. In an additional testament to the versatility of this approach, functionalization of the amino groups on the organic linkers was achieved by incorporating

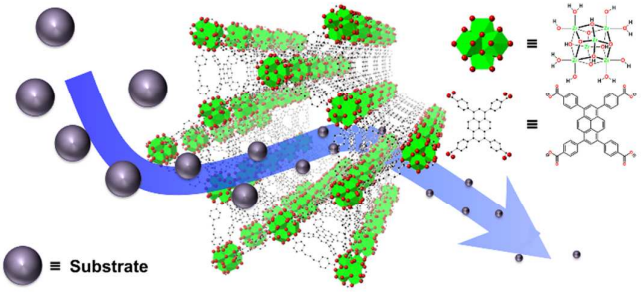

Figure 6. Schematic representing diffusion of a substrate through a NU-1000 NMOF crystallite. Small particle sizes afford larger external surface areas and rapid access to internal catalytic active sites by reducing reactant and product diffusion rates.

either acetic acid or fluorescein isothiocyanate in the reaction to yield functionalized NMOFs ca. 100–150 nm or 20–30 nm in diameter, respectively (although reproducible small particles were observed in this work, it remains unclear as to why the fluorescein derivatives are so much smaller than the unfunctionalized analogs).

3. Select applications of NMOFs

3.1 Catalysis

Employing the metal node and/or organic linker of a MOF as a catalyst or catalyst support is of interest due to the ability to achieve site-isolated catalytic activity of controlled composition.[30] Furthermore, while the permanent porosity of MOFs is advantageous for catalytic applications, accessibility of the active sites can still be a challenge, especially if the catalytic reactions involve large substrates that suffer from increased diffusion rates to internal catalytic sites (Figure 6). One way to accelerate the diffusion of substrates and/or products in a catalytic MOF material is to synthesize NMOFs, which feature greater external surface area and lower diffusion barriers.

Li *et al.* have reported the modulator controlled solvothermal synthesis of nano-sized NU-1000 (Section 2.1), a Zr-based mesoporous MOF, and demonstrated the effect of crystallite size on hydrolysis of a nerve agent simulant, dimethyl 4-nitrophenylphosphate (DMNP).[60] As expected, catalytic activity increased significantly upon decreasing crystallite size since, intuitively, the smaller particles demonstrate larger external surface areas (enabling access to more surface-based catalytic sites) and facilitate faster access to the Zr_6-nodal active sites within NU-1000. In a related example, Li *et al.* also designed a Zr-based MOF, NU-1003, that possesses large mesopores (ca. 4.5 nm) which allow for the immobilization of the nerve agent hydrolyzing enzyme, organophosphorus acid anhydrolase (OPAA).[61] In addition to designing a MOF with large pores for enzyme encapsulation, NU-1003 was also prepared on the nanometer scale to facilitate faster diffusion of the nerve agent, soman (GD) throughout the MOF-enzyme composite. The nano-sized enzyme carrier not only led to enhanced stability of the enzyme but due to enhanced diffusion, the composite activity was found to exceed that of the free enzyme. It should be noted that maintaining or exceeding the activity of free enzymes with composite materials is a challenging task.[155, 156] The use of nano-sized MOF-enzyme systems is of particular interest for biomedical applications where the size of crystallites can be crucial for achieving facile transport through the circulatory system as well as allowing for cellular uptake.

While many NMOFs can be synthesized to have monodisperse particle sizes, there are still many more MOFs that have been shown to crystallize in a polydisperse fashion. Given that the size of the NMOF crystallite has significant implications with respect to catalytic competence, it is important to ensure that samples contain monodisperse particle sizes before drawing conclusions about catalytic activity. The importance of particle monodispersity was illustrated by Janiak *et al.* in a study where the Brønsted acidity of 2-nitro-, and 2-amino-terephthalate-functionalized MIL-101Cr NMOFs was leveraged to catalyse diacetilization of benzaldehyde with methanol.[157] Nano-regime MOF particles (<200 nm in this example) were determined to be the primary contributor to catalytic reactivity after removal (by filtration) of the bulk MOF particles from the reaction mixture and post leaching analysis. It was found that the nano-sized MOF particles were responsible for ca. 67% of the observed overall activity despite much lower molar amounts of NMOF being present in the mixture. Perhaps more significantly, less than 1 mg of NMOF 2-nitro-MIL-101Cr (particle diameters of 245 ± 117 nm) isolated from the bulk 2-nitro-MIL-101Cr sample through ultracentrifugation was found to enable a conversion of 68% (90 min reaction) where 10 mg of a bulk sample of nonfunctionalized MIL-101Cr (particle diameters of 479 ± 150 nm) produces nearly the same conversion (albeit with comparable turnover frequencies and numbers). While the Brønsted acidity of the functional group on the linker is expected to play a significant role in this catalysis (hence the higher catalytic activity of the nitro-substituted frameworks), it was also determined that a comparable increase in activity was observed when the particle size of the amino-functionalized MIL-101Cr was decreased, unequivocally providing evidence for particle-size enhancements independent of framework functionalization.

3.2 Sensing and Imaging

MOFs have been studied for their potential in sensing applications and as alternative materials to metal-oxide, nanoparticulate, and quantum-dot based sensors.[158] Rieter and coworkers have shown that nano-sized Gd(III)-based MOFs prepared via (water-in-oil) microemulsion methods (Figure 7) can be utilized as contrast agents for magnetic resonance imaging (MRI) where the paramagnetic nature of Gd(III) ions improve image contrast by increasing water proton relaxation rates.[159] Gd(III)-based MOF nanorods (ranging in length from 100–1000 nm and in diameter from 40–100 nm), as positive (T_1-weighted) contrast agents, demonstrate an order of magnitude of enhancement in relaxivity ($R1 \approx 1.6 \times 10^7\ s^{-1}$ per mM of nanorod) compared to Gd(III)-bearing liposomes and Omniscan™ (gadodiamide), a clinically used small molecule contrast agent. Size-dependent relaxivity values were observed where nano-sized MOF particles showed larger relaxivity values attributed to higher Gd-bound water exchange rates due to large surface-to-volume ratios of the particles, suggesting that Gd(III) centers near the surface are primarily responsible for the enhancement. As expected, increasing the nanorod size results in an inverse size dependence in relaxitivity (per mM Gd).

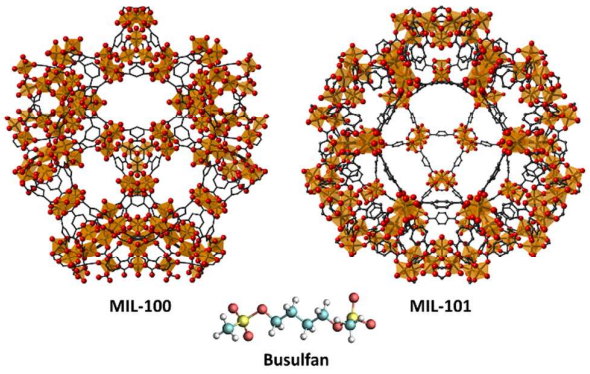

Figure 8. Structures of Fe-based MIL-100, MIL-101 and anti-cancer drug Busulfan. Busulfan@MIL-100 composite has been found to retain the activity of Busulfan with respect to human leukemia and multiple myeloma. Adapted from ref. 96.

Using a reverse microemulsion approach, Rieter *et al.* synthesized Ln-MOF@SiO_2, Ln = Eu(III), Gd(III), Tb(III), core-shell adducts via Ln-MOF nanoparticles functionalized with polyvinylpyrrolidone (PVP). The PVP coated NMOFs were prepared in a nanorod morphology (ca. 100 nm in length, 40 nm in width) while the subsequently prepared silica coated particles had silica shells ranging in thickness from 2–9 nm (dependent on the reaction time employed in the sol-gel preparation method). While guarding the NMOF against dissolution, the silica shell of a Eu-doped Gd-NMOF was functionalized with a silated Tb-derivative to afford luminescence sensing of dipicolinic acid (DPA), a major component of bacterial endospores, with a detection limit of ~48 nM.[160] In a somewhat related example, Xu *et al.* showed that highly selective luminescence sensing of DPA, in the presence of other carboxylic acid based aromatic compounds and inorganic anions, is enhanced by using nano-sized Eu(III)-fumarate-oxalate-based NMOFs (200–400 nm) prepared by a microemulsion method.[161] Upon increasing the amount of CTAB added during MOF preparation, particle sizes decreased from the macro regime (2–4 μm) to the nano. Perhaps most significantly, it was determined that the Bravais–Friedel–Donnay–Harker (BFDH) method can be applied to this synthetic scheme to simulate crystallite growth and predict morphology with reasonable accuracy opening the door to predictive synthetic methodologies where specific nanomorphologies and crystallite sizes can be targeted depending on the desired application.

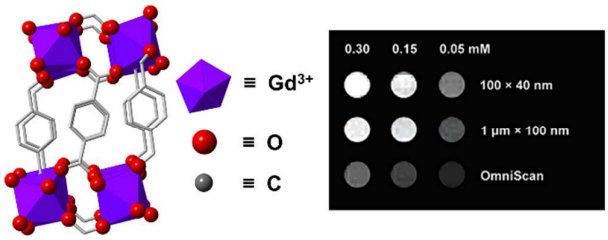

Figure 7. Structure and T1-weighted magnetic resonance images of suspensions of $Gd(BDC)_{1.5}(H_2O)_2$ crystallites obtained from different water/surfactant molar ratios. Reprinted with permission from W. J. Rieter *et al. J. Am. Chem. Soc.*, 2006, **128**, 9024-9025. Copyright 2006 American Chemical Society.

3.3 Drug Delivery

Nano-sized MOFs have gained significant attention as non-toxic nanocarriers which have the potential to overcome issues associated with low drug loading and/or payload loss through leaching.[162] Horcajada *et al.* have shown that iron carboxylate based nano-sized MIL MOFs (with mean diameters <200 nm) prepared via conventional solvothermal or microwave synthetic methods can be employed for the encapsulation of challenging therapeutic agents as biocompatible nanocarriers (where the cytotoxicity of the NMOFs was determined to be comparable to that observed for other conventional nanoparticulate delivery systems).[96] In one representative example from this wide ranging study, nanosized MIL-100 was shown to adsorb 25 wt% busulfan (an anticancer drug, Figure 8), representing a loading that is 5-fold higher than that of known polymer nanoparticles, and marks a 60-fold enhancement over liposome loading. Busulfan is a particularly challenging chemotherapy target owing to its poor stability in aqueous solution and hepatic toxicity. Achieving high loading of a target drug in a nanocarrier is crucial since it facilitates the use of lower amounts of the carrier material to deliver the needed dose (actual intravenous dosage of MIL-100 encapsulating busulfan is anticipated to be around 20 mg kg^{-1} and avoid the use organic solvents such as *N,N'*-dimethylacetamide reducing hepatic toxicity). Importantly, the activity of the busulfan@MIL-100 composite was tested against human leukemia and human multiple myeloma cells resulting in the preservation of the activity of busulfan (where the activity was the same as that observed for the free busulfan) with a total absence of MIL-100 cytotoxicity. To further confirm the biodegradability and cytotoxicity of NMOF nanocarriers, Baati *et al.* performed *in vivo* toxicity experiments in rats using the same Fe(III)-based nanosized MILs.[163] Low acute toxicity was confirmed and the MOF nanoparticles were rapidly sequestered in the liver and spleen. Components of the NMOFs such as iron and organic linkers were subsequently detected in urine and feces samples.

One potential approach to using NMOFs in therapeutic applications involves the preparation of MOFs that incorporate photosensitizer-based organic linkers to generate singlet oxygen (a prerequisite of photodynamic therapy). To avoid non-productive excited state deactivation through chromophore aggregation, MOFs may be used to facilitate a rigid spatial distribution of immobilized photosensitizers. To this end, porphyrin-based PCN-222/MOF-545 NMOFs (with average sizes ranging from 50–800 nm) prepared via acetic acid modulator controlled solvothermal methods have been evaluated in the context of photodynamic therapy.[164] Cellular uptake (with HeLa cells) experiments with these materials determined that larger particles were bound to cell membranes but less efficiently internalized than smaller crystallites. No size-dependent preference for association of NMOFs with cells was apparent from confocal microscopy analysis. In these materials, superior phototoxicity of the

NMOFs over the free linkers is attributed to the controlled mechanism of tumor cell apoptosis due to oxidative stress in the former while the latter predominantly causes traumatic cell death. Serendipitously, NMOF decomposition in biological media (stability of Zr-based MOFs in the presence of phosphates is a known shortcoming) after 20 h in cells leads to a deactivation of phototoxicity affording an auspicious pathway for eliminating post-treatment issues.

4. Conclusions and Outlook

Although all the synthetic methods described herein may be used to generate NMOFs, it is clear that no one synthetic strategy is all encompassing. Solvothermal methods offer the greatest flexibility in terms of linker selection as practical solubility considerations can be overcome with judicious reaction condition selection. This comes at the cost of long reaction times, the need for systematic optimization of reaction conditions to improve crystallite polydispersity, and rudimentary (albeit well understood) control over crystallite size. Sonochemical and microwave methods improve on the logistical aspects of solvothermal syntheses with shorter and controlled reaction times, often at the cost of scalability. Meanwhile, surfactant-mediated and microemulsion type methodologies offer the possibility for hierarchical design of composite MOF materials, where control over the long-range hierarchy is exercised through the nature of the templating micelles formed as part of the emulsification process. However, solubility considerations greatly limit the applicability of this approach, as large organic linkers often require common organic solvents for dissolution and are sparingly, or not at all soluble in water and ethanol, obviating the possibility for synthesis within the water phase of the microemulsion.

The use of smaller particle sizes engenders many advantages in potential applications. Increased external surface areas coupled with shorter diffusion pathways for reactants, mediators and products translate to improvements in catalytic reactions. Conversely, small particle sizes are often desirable for biomedical applications where molecular drug delivery and imaging systems must traverse a complex physiological roadmap where vessels, tissue, and biological membranes all have varying levels of permeability. Thus, the retained porosity of NMOF crystallites must be leveraged to store and protect payloads while the small crystallite size facilitates biological transport and in some cases biodegradability. One additional consideration is control over particle nanomorphology. While discussion of morphology falls outside of the scope of this overview, it stands to reason that varying the morphology of the crystallites discussed in this overview (from rods to plates, for example) will also impact the performance of these materials in many of these applications.

It is clear that efforts to optimize size-controlled syntheses of MOFs are of importance, particularly due to the multitude of applications that benefit from the inherent properties of smaller crystallites. Many recent studies have confirmed the unique utility of NMOFs, and we firmly believe that there are still many potential applications that remain underexplored. ·

Conflicts of interest

There are no conflicts to declare.

Acknowledgements

OKF gratefully acknowledges support by the DOE Separations and Analysis Program funded by the U.S. Department of Energy, Office of Science (Awards DE-FG02−08ER15967) and Defense Threat Reduction Agency (HDTRA1-18-1-0003). HN gratefully acknowledges support from the Ryan Fellowship and the Northwestern University International Institute of Nanotechnology.

Notes and references

1. For the purposes of the discussion in this review, we will consider crystallites in this size regime (5-500 nm) as "nano-sized." We do, however, note that the widely accepted size range definition of nanoscale particles is 1-100 nm.
2. S. Mintova, M. Jaber and V. Valtchev, *Chem. Soc. Rev.*, 2015, **44**, 7207-7233.
3. A. P. Alivisatos, *Science*, 1996, **271**, 933-937.
4. X. Peng, M. C. Schlamp, A. V. Kadavanich and A. P. Alivisatos, *J. Am. Chem. Soc.*, 1997, **119**, 7019-7029.
5. T. Trindade, P. O'Brien and N. L. Pickett, *Chem. Mater.*, 2001, **13**, 3843-3858.
6. M. Haruta, N. Yamada, T. Kobayashi and S. Iijima, *J. Catal.*, 1989, **115**, 301-309.
7. M. Valden, X. Lai and D. W. Goodman, *Science*, 1998, **281**, 1647-1650.
8. A. Aharoni, T. Mokari, I. Popov and U. Banin, *J. Am. Chem. Soc.*, 2006, **128**, 257-264.
9. I. Potapova, R. Mruk, C. Hübner, R. Zentel, T. Basché and A. Mews, *Angew. Chem. Int. Ed.*, 2005, **44**, 2437-2440.
10. D. Wang, T. Xie and Y. Li, *Nano Research*, 2009, **2**, 30-46.
11. D. Wang and Y. Li, *Adv. Mater.*, 2011, **23**, 1044-1060.
12. X. Peng, L. Manna, W. Yang, J. Wickham, E. Scher, A. Kadavanich and A. P. Alivisatos, *Nature*, 2000, **404**, 59-61.
13. A. H. Mueller, M. A. Petruska, M. Achermann, D. J. Werder, E. A. Akhadov, D. D. Koleske, M. A. Hoffbauer and V. I. Klimov, *Nano Lett.*, 2005, **5**, 1039-1044.
14. B. N. Pal, Y. Ghosh, S. Brovelli, R. Laocharoensuk, V. I. Klimov, J. A. Hollingsworth and H. Htoon, *Nano Lett.*, 2012, **12**, 331-336.
15. Y. Liang, Y. Li, H. Wang, J. Zhou, J. Wang, T. Regier and H. Dai, *Nat Mater*, 2011, **10**, 780-786.
16. N. Bao, L. Shen, T. Takata and K. Domen, *Chem. Mater.*, 2008, **20**, 110-117.
17. C.-K. Tsung, J. N. Kuhn, W. Huang, C. Aliaga, L.-I. Hung, G. A. Somorjai and P. Yang, *J. Am. Chem. Soc.*, 2009, **131**, 5816-5822.
18. S. E. Habas, H. Lee, V. Radmilovic, G. A. Somorjai and P. Yang, *Nat Mater*, 2007, **6**, 692-697.

19. Y. Yin, R. M. Rioux, C. K. Erdonmez, S. Hughes, G. A. Somorjai and A. P. Alivisatos, *Science*, 2004, **304**, 711-714.
20. K. Zhou and Y. Li, *Angew. Chem. Int. Ed.*, 2012, **51**, 602-613.
21. Y. Zheng, X. Li and P. K. Dutta, *Sensors*, 2012, **12**, 5170.
22. H. Li, W. Cheng, Y. Wang, B. Liu, W. Zhang and H. Zhang, *Chem. Eur. J.*, 2010, **16**, 2125-2130.
23. M. Zaarour, B. Dong, I. Naydenova, R. Retoux and S. Mintova, *Microporous Mesoporous Mater.*, 2014, **189**, 11-21.
24. W. Shan, T. Yu, B. Wang, J. Hu, Y. Zhang, X. Wang and Y. Tang, *Chem. Mater.*, 2006, **18**, 3169-3172.
25. C. Platas-Iglesias, L. Vander Elst, W. Zhou, R. N. Muller, C. F. G. C. Geraldes, T. Maschmeyer and J. A. Peters, *Chem. Eur. J.*, 2002, **8**, 5121-5131.
26. T. Yu, Y. Zhang, C. You, J. Zhuang, B. Wang, B. Liu, Y. Kang and Y. Tang, *Chem. Eur. J.*, 2006, **12**, 1137-1143.
27. H. Li, M. Eddaoudi, M. O'Keeffe and O. M. Yaghi, *Nature*, 1999, **402**, 276-279.
28. N. L. Rosi, J. Eckert, M. Eddaoudi, D. T. Vodak, J. Kim, M. O'Keeffe and O. M. Yaghi, *Science*, 2003, **300**, 1127-1129.
29. S. Kitagawa, R. Kitaura and S.-i. Noro, *Angew. Chem. Int. Ed.*, 2004, **43**, 2334-2375.
30. T. Islamoglu, S. Goswami, Z. Li, A. J. Howarth, O. K. Farha and J. T. Hupp, *Acc. Chem. Res.*, 2017, **50**, 805-813.
31. J.-R. Li, R. J. Kuppler and H.-C. Zhou, *Chem. Soc. Rev.*, 2009, **38**, 1477-1504.
32. L. J. Murray, M. Dinca and J. R. Long, *Chem. Soc. Rev.*, 2009, **38**, 1294-1314.
33. J. Lee, O. K. Farha, J. Roberts, K. A. Scheidt, S. T. Nguyen and J. T. Hupp, *Chem. Soc. Rev.*, 2009, **38**, 1450-1459.
34. H. Furukawa, Y. B. Go, N. Ko, Y. K. Park, F. J. Uribe-Romo, J. Kim, M. O'Keeffe and O. M. Yaghi, *Inorg. Chem.*, 2011, **50**, 9147-9152.
35. D. Gygi, E. D. Bloch, J. A. Mason, M. R. Hudson, M. I. Gonzalez, R. L. Siegelman, T. A. Darwish, W. L. Queen, C. M. Brown and J. R. Long, *Chem. Mater.*, 2016, **28**, 1128-1138.
36. Y. Liao, L. Zhang, M. H. Weston, W. Morris, J. T. Hupp and O. K. Farha, *Chem. Commun.*, 2017, **53**, 9376-9379.
37. H. Deng, S. Grunder, K. E. Cordova, C. Valente, H. Furukawa, M. Hmadeh, F. Gándara, A. C. Whalley, Z. Liu, S. Asahina, H. Kazumori, M. O'Keeffe, O. Terasaki, J. F. Stoddart and O. M. Yaghi, *Science*, 2012, **336**, 1018-1023.
38. D. A. Gómez-Gualdrón, T. C. Wang, P. García-Holley, R. M. Sawelewa, E. Argueta, R. Q. Snurr, J. T. Hupp, T. Yildirim and O. K. Farha, *ACS Appl. Mater. Interfaces*, 2017, **9**, 33419-33428.
39. H. Fei, S. Pullen, A. Wagner, S. Ott and S. M. Cohen, *Chem. Commun.*, 2015, **51**, 66-69.
40. H. Fei and S. M. Cohen, *J. Am. Chem. Soc.*, 2015, **137**, 2191-2194.
41. M. Rimoldi, A. Nakamura, N. A. Vermeulen, J. J. Henkelis, A. K. Blackburn, J. T. Hupp, J. F. Stoddart and O. K. Farha, *Chem. Sci.*, 2016, **7**, 4980-4984.
42. I. Hod, W. Bury, D. M. Gardner, P. Deria, V. Roznyatovskiy, M. R. Wasielewski, O. K. Farha and J. T. Hupp, *J. Phys. Chem. Lett.*, 2015, **6**, 586-591.
43. O. V. Gutov, M. G. Hevia, E. C. Escudero-Adán and A. Shafir, *Inorg. Chem.*, 2015, **54**, 8396-8400.
44. H. Noh, Y. Cui, A. W. Peters, D. R. Pahls, M. A. Ortuño, N. A. Vermeulen, C. J. Cramer, L. Gagliardi, J. T. Hupp and O. K. Farha, *J. Am. Chem. Soc.*, 2016, **138**, 14720-14726.
45. Z. Li, N. M. Schweitzer, A. B. League, V. Bernales, A. W. Peters, A. B. Getsoian, T. C. Wang, J. T. Miller, A. Vjunov, J. L. Fulton, J. A. Lercher, C. J. Cramer, L. Gagliardi, J. T. Hupp and O. K. Farha, *J. Am. Chem. Soc.*, 2016, **138**, 1977-1982.
46. S. Ahn, N. E. Thornburg, Z. Li, T. C. Wang, L. C. Gallington, K. W. Chapman, J. M. Notestein, J. T. Hupp and O. K. Farha, *Inorg. Chem.*, 2016, **55**, 11954-11961.
47. A. W. Peters, Z. Li, O. K. Farha and J. T. Hupp, *ACS Nano*, 2015, **9**, 8484-8490.
48. A. W. Peters, Z. Li, O. K. Farha and J. T. Hupp, *ACS Appl. Mater. Interfaces*, 2016, **8**, 20675-20681.
49. J. E. Mondloch, W. Bury, D. Fairen-Jimenez, S. Kwon, E. J. DeMarco, M. H. Weston, A. A. Sarjeant, S. T. Nguyen, P. C. Stair, R. Q. Snurr, O. K. Farha and J. T. Hupp, *J. Am. Chem. Soc.*, 2013, **135**, 10294-10297.
50. A. E. Platero-Prats, A. B. League, V. Bernales, J. Ye, L. C. Gallington, A. Vjunov, N. M. Schweitzer, Z. Li, J. Zheng, B. L. Mehdi, A. J. Stevens, A. Dohnalkova, M. Balasubramanian, O. K. Farha, J. T. Hupp, N. D. Browning, J. L. Fulton, D. M. Camaioni, J. A. Lercher, D. G. Truhlar, L. Gagliardi, C. J. Cramer and K. W. Chapman, *J. Am. Chem. Soc.*, 2017, **139**, 10410-10418.
51. Z. Li, A. W. Peters, V. Bernales, M. A. Ortuño, N. M. Schweitzer, M. R. DeStefano, L. C. Gallington, A. E. Platero-Prats, K. W. Chapman, C. J. Cramer, L. Gagliardi, J. T. Hupp and O. K. Farha, *ACS Cent. Sci.*, 2017, **3**, 31-38.
52. M. Rimoldi, V. Bernales, J. Borycz, A. Vjunov, L. C. Gallington, A. E. Platero-Prats, I. S. Kim, J. L. Fulton, A. B. F. Martinson, J. A. Lercher, K. W. Chapman, C. J. Cramer, L. Gagliardi, J. T. Hupp and O. K. Farha, *Chem. Mater.*, 2017, **29**, 1058-1068.
53. C.-W. Kung, J. E. Mondloch, T. C. Wang, W. Bury, W. Hoffeditz, B. M. Klahr, R. C. Klet, M. J. Pellin, O. K. Farha and J. T. Hupp, *ACS Appl. Mater. Interfaces*, 2015, **7**, 28223-28230.
54. Y. K. Hwang, D.-Y. Hong, J.-S. Chang, S. H. Jhung, Y.-K. Seo, J. Kim, A. Vimont, M. Daturi, C. Serre and G. Férey, *Angew. Chem. Int. Ed.*, 2008, **47**, 4144-4148.
55. S. Choi, T. Watanabe, T.-H. Bae, D. S. Sholl and C. W. Jones, *J. Phys. Chem. Lett.*, 2012, **3**, 1136-1141.
56. R. L. Siegelman, T. M. McDonald, M. I. Gonzalez, J. D. Martell, P. J. Milner, J. A. Mason, A. H. Berger, A. S. Bhown and J. R. Long, *J. Am. Chem. Soc.*, 2017, **139**, 10526-10538.
57. P. Deria, W. Bury, J. T. Hupp and O. K. Farha, *Chem. Commun.*, 2014, **50**, 1965-1968.
58. P. Deria, J. E. Mondloch, E. Tylianakis, P. Ghosh, W. Bury, R. Q. Snurr, J. T. Hupp and O. K. Farha, *J. Am. Chem. Soc.*, 2013, **135**, 16801-16804.
59. A. J. Howarth, C. T. Buru, Y. Liu, A. M. Ploskonka, K. J. Hartlieb, M. McEntee, J. J. Mahle, J. H. Buchanan, E. M. Durke, S. S. Al-Juaid, J. F. Stoddart, J. B. DeCoste, J. T. Hupp and O. K. Farha, *Chem. Eur. J.*, 2017, **23**, 214-218.
60. P. Li, R. C. Klet, S.-Y. Moon, T. C. Wang, P. Deria, A. W. Peters, B. M. Klahr, H.-J. Park, S. S. Al-Juaid, J. T. Hupp and O. K. Farha, *Chem. Commun.*, 2015, **51**, 10925-10928.
61. P. Li, S.-Y. Moon, M. A. Guelta, L. Lin, D. A. Gómez-Gualdrón, R. Q. Snurr, S. P. Harvey, J. T. Hupp and O. K. Farha, *ACS Nano*, 2016, **10**, 9174-9182.

62. C. Doonan, R. Riccò, K. Liang, D. Bradshaw and P. Falcaro, *Acc. Chem. Res.*, 2017, **50**, 1423-1432.
63. D. Feng, T.-F. Liu, J. Su, M. Bosch, Z. Wei, W. Wan, D. Yuan, Y.-P. Chen, X. Wang, K. Wang, X. Lian, Z.-Y. Gu, J. Park, X. Zou and H.-C. Zhou, *Nat. Commun.*, 2015, **6**, 5979.
64. Y. He, W. Zhou, T. Yildirim and B. Chen, *Energy Environ. Sci.*, 2013, **6**, 2735-2744.
65. U. Stoeck, S. Krause, V. Bon, I. Senkovska and S. Kaskel, *Chem. Commun.*, 2012, **48**, 10841-10843.
66. U. Stoeck, I. Senkovska, V. Bon, S. Krause and S. Kaskel, *Chem. Commun.*, 2015, **51**, 1046-1049.
67. M. J. Katz, A. J. Howarth, P. Z. Moghadam, J. B. DeCoste, R. Q. Snurr, J. T. Hupp and O. K. Farha, *Dalton Trans.*, 2016, **45**, 4150-4153.
68. C. O. Audu, H. G. T. Nguyen, C.-Y. Chang, M. J. Katz, L. Mao, O. K. Farha, J. T. Hupp and S. T. Nguyen, *Chem. Sci.*, 2016, **7**, 6492-6498.
69. Y.-S. Bae, C. Y. Lee, K. C. Kim, O. K. Farha, P. Nickias, J. T. Hupp, S. T. Nguyen and R. Q. Snurr, *Angew. Chem. Int. Ed.*, 2012, **51**, 1857-1860.
70. Y. G. Chung, P. Bai, M. Haranczyk, K. T. Leperi, P. Li, H. Zhang, T. C. Wang, T. Duerinck, F. You, J. T. Hupp, O. K. Farha, J. I. Siepmann and R. Q. Snurr, *Chem. Mater.*, 2017, **29**, 6315-6328.
71. A. J. Howarth, M. J. Katz, T. C. Wang, A. E. Platero-Prats, K. W. Chapman, J. T. Hupp and O. K. Farha, *J. Am. Chem. Soc.*, 2015, **137**, 7488-7494.
72. B. Chen, C. Liang, J. Yang, D. S. Contreras, Y. L. Clancy, E. B. Lobkovsky, O. M. Yaghi and S. Dai, *Angew. Chem.*, 2006, **118**, 1418-1421.
73. Z. R. Herm, E. D. Bloch and J. R. Long, *Chem. Mater.*, 2014, **26**, 323-338.
74. C. Wang, D. Liu and W. Lin, *J. Am. Chem. Soc.*, 2013, **135**, 13222-13234.
75. J. Zhang, Z. Li, W. Gong, X. Han, Y. Liu and Y. Cui, *Inorg. Chem.*, 2016, **55**, 7229-7232.
76. C. Y. Lee, O. K. Farha, B. J. Hong, A. A. Sarjeant, S. T. Nguyen and J. T. Hupp, *J. Am. Chem. Soc.*, 2011, **133**, 15858-15861.
77. J.-L. Wang, C. Wang and W. Lin, *ACS Catal.*, 2012, **2**, 2630-2640.
78. H.-J. Son, S. Jin, S. Patwardhan, S. J. Wezenberg, N. C. Jeong, M. So, C. E. Wilmer, A. A. Sarjeant, G. C. Schatz, R. Q. Snurr, O. K. Farha, G. P. Wiederrecht and J. T. Hupp, *J. Am. Chem. Soc.*, 2013, **135**, 862-869.
79. M. E. Foster, J. D. Azoulay, B. M. Wong and M. D. Allendorf, *Chem. Sci.*, 2014, **5**, 2081-2090.
80. V. Stavila, A. A. Talin and M. D. Allendorf, *Chem. Soc. Rev.*, 2014, **43**, 5994-6010.
81. B. Chen, L. Wang, Y. Xiao, F. R. Fronczek, M. Xue, Y. Cui and G. Qian, *Angew. Chem. Int. Ed.*, 2009, **48**, 500-503.
82. M. D. Allendorf, R. J. T. Houk, L. Andruszkiewicz, A. A. Talin, J. Pikarsky, A. Choudhury, K. A. Gall and P. J. Hesketh, *J. Am. Chem. Soc.*, 2008, **130**, 14404-14405.
83. Z. Hu, B. J. Deibert and J. Li, *Chem. Soc. Rev.*, 2014, **43**, 5815-5840.
84. G. Lu and Joseph T. Hupp, *J. Am. Chem. Soc.*, 2010, **132**, 7832-7833.
85. L. E. Kreno, K. Leong, Omar K. Farha, M. D. Allendorf, R. P. Van Duyne and Joseph T. Hupp, *Chem. Rev.*, 2011, **112**, 1105-1125.
86. Y. Liu, Y. Ban and W. Yang, *Adv. Mater.*, 2017, **29**, 1606949.
87. N. Rangnekar, N. Mittal, B. Elyassi, J. Caro and M. Tsapatsis, *Chem. Soc. Rev.*, 2015, **44**, 7128-7154.
88. Y. Peng, Y. Li, Y. Ban, H. Jin, W. Jiao, X. Liu and W. Yang, *Science*, 2014, **346**, 1356-1359.
89. Z. Y. Yeo, S.-P. Chai, P. W. Zhu and A. R. Mohamed, *RSC Adv.*, 2014, **4**, 54322-54334.
90. L. Dong, M. Chen, J. Li, D. Shi, W. Dong, X. Li and Y. Bai, *J. Membr. Sci.*, 2016, **520**, 801-811.
91. W. Chen and C. Wu, *Dalton Trans.*, 2018, **47**, 2114-2133.
92. A. C. McKinlay, R. E. Morris, P. Horcajada, G. Férey, R. Gref, P. Couvreur and C. Serre, *Angew. Chem. Int. Ed.*, 2010, **49**, 6260-6266.
93. N. J. Hinks, A. C. McKinlay, B. Xiao, P. S. Wheatley and R. E. Morris, *Microporous Mesoporous Mater.*, 2010, **129**, 330-334.
94. B. F. Abrahams, B. F. Hoskins, D. M. Michail and R. Robson, *Nature*, 1994, **369**, 727.
95. O. M. Yaghi, G. Li and H. Li, *Nature*, 1995, **378**, 703.
96. P. Horcajada, T. Chalati, C. Serre, B. Gillet, C. Sebrie, T. Baati, J. F. Eubank, D. Heurtaux, P. Clayette, C. Kreuz, J.-S. Chang, Y. K. Hwang, V. Marsaud, P.-N. Bories, L. Cynober, S. Gil, G. Ferey, P. Couvreur and R. Gref, *Nat Mater*, 2010, **9**, 172-178.
97. W. Morris, W. E. Briley, E. Auyeung, M. D. Cabezas and C. A. Mirkin, *J. Am. Chem. Soc.*, 2014, **136**, 7261-7264.
98. C. He, K. Lu, D. Liu and W. Lin, *J. Am. Chem. Soc.*, 2014, **136**, 5181-5184.
99. S. Wang, W. Morris, Y. Liu, C. M. McGuirk, Y. Zhou, J. T. Hupp, O. K. Farha and C. A. Mirkin, *Angew. Chem. Int. Ed.*, 2015, **54**, 14738-14742.
100. E. A. Flugel, A. Ranft, F. Haase and B. V. Lotsch, *J. Mater. Chem.*, 2012, **22**, 10119-10133.
101. A. Carne, C. Carbonell, I. Imaz and D. Maspoch, *Chem. Soc. Rev.*, 2011, **40**, 291-305.
102. A. M. Spokoyny, D. Kim, A. Sumrein and C. A. Mirkin, *Chem. Soc. Rev.*, 2009, **38**, 1218-1227.
103. N. Stock and S. Biswas, *Chem. Rev.*, 2012, **112**, 933-969.
104. A. J. Howarth, A. W. Peters, N. A. Vermeulen, T. C. Wang, J. T. Hupp and O. K. Farha, *Chem. Mater.*, 2017, **29**, 26-39.
105. H. Bunzen, M. Grzywa, M. Hambach, S. Spirkl and D. Volkmer, *Cryst. Growth Des.*, 2016, **16**, 3190-3197.
106. J. Cravillon, S. Münzer, S.-J. Lohmeier, A. Feldhoff, K. Huber and M. Wiebcke, *Chem. Mater.*, 2009, **21**, 1410-1412.
107. Y. Pan, Y. Liu, G. Zeng, L. Zhao and Z. Lai, *Chem. Commun.*, 2011, **47**, 2071-2073.
108. W. Xia, J. Zhu, W. Guo, L. An, D. Xia and R. Zou, *J. Mater. Chem. A*, 2014, **2**, 11606-11613.
109. X. Lan, N. Huang, J. Wang and T. Wang, *Chem. Commun.*, 2018, **54**, 584-587.
110. S. Diring, S. Furukawa, Y. Takashima, T. Tsuruoka and S. Kitagawa, *Chem. Mater.*, 2010, **22**, 4531-4538.
111. M. R. DeStefano, T. Islamoglu, S. J. Garibay, J. T. Hupp and O. K. Farha, *Chem. Mater.*, 2017, **29**, 1357-1361.
112. H. Wu, Y. S. Chua, V. Krungleviciute, M. Tyagi, P. Chen, T. Yildirim and W. Zhou, *J. Am. Chem. Soc.*, 2013, **135**, 10525-10532.
113. A. Schaate, P. Roy, A. Godt, J. Lippke, F. Waltz, M. Wiebcke and P. Behrens, *Chem. Eur. J.*, 2011, **17**, 6643-6651.

114. M. J. Katz, Z. J. Brown, Y. J. Colon, P. W. Siu, K. A. Scheidt, R. Q. Snurr, J. T. Hupp and O. K. Farha, *Chem. Commun.*, 2013, **49**, 9449-9451.
115. W. Morris, S. Wang, D. Cho, E. Auyeung, P. Li, O. K. Farha and C. A. Mirkin, *ACS Appl. Mater. Interfaces*, 2017, **9**, 33413-33418.
116. S. Hu, M. Liu, X. Guo, K. Li, Y. Han, C. Song and G. Zhang, *Cryst. Growth Des.*, 2017, **17**, 6586-6595.
117. N. A. Khan and S. H. Jhung, *Coord. Chem. Rev.*, 2015, **285**, 11-23.
118. J. Klinowski, F. A. Almeida Paz, P. Silva and J. Rocha, *Dalton Trans.*, 2011, **40**, 321-330.
119. N. A. Khan, J. W. Jun and S. H. Jhung, *Eur. J. Inorg. Chem.*, 2010, **2010**, 1043-1048.
120. Y.-S. Bae, K. L. Mulfort, H. Frost, P. Ryan, S. Punnathanam, L. J. Broadbelt, J. T. Hupp and R. Q. Snurr, *Langmuir*, 2008, **24**, 8592-8598.
121. P. Amo-Ochoa, G. Givaja, P. J. S. Miguel, O. Castillo and F. Zamora, *Inorg. Chem. Commun.*, 2007, **10**, 921-924.
122. Y.-K. Seo, G. Hundal, I. T. Jang, Y. K. Hwang, C.-H. Jun and J.-S. Chang, *Microporous Mesoporous Mater.*, 2009, **119**, 331-337.
123. J.-S. Choi, W.-J. Son, J. Kim and W.-S. Ahn, *Microporous Mesoporous Mater.*, 2008, **116**, 727-731.
124. M. Taddei, P. V. Dau, S. M. Cohen, M. Ranocchiari, J. A. van Bokhoven, F. Costantino, S. Sabatini and R. Vivani, *Dalton Trans.*, 2015, **44**, 14019-14026.
125. K. S. Suslick, *Science*, 1990, **247**, 1439-1445.
126. M. Bigdeli and A. Morsali, *Ultrason. Sonochem.*, 2015, **27**, 416-422.
127. C. G. Carson, A. J. Brown, D. S. Sholl and S. Nair, *Cryst. Growth Des.*, 2011, **11**, 4505-4510.
128. D.-W. Jung, D.-A. Yang, J. Kim, J. Kim and W.-S. Ahn, *Dalton Trans.*, 2010, **39**, 2883-2887.
129. W.-J. Son, J. Kim, J. Kim and W.-S. Ahn, *Chem. Commun.*, 2008, **0**, 6336-6338.
130. B. Seoane, J. M. Zamaro, C. Tellez and J. Coronas, *CrystEngComm*, 2012, **14**, 3103-3107.
131. Z.-Q. Li, A. Wang, C.-Y. Guo, Y.-F. Tai and L.-G. Qiu, *Dalton Trans.*, 2013, **42**, 13948-13954.
132. C. Gao, Y. Sakamoto, O. Terasaki, K. Sakamoto and S. Che, *J. Mater. Chem.*, 2007, **17**, 3591-3602.
133. W. Park, D. Yu, K. Na, K. E. Jelfs, B. Slater, Y. Sakamoto and R. Ryoo, *Chem. Mater.*, 2011, **23**, 5131-5137.
134. K. Cho, K. Na, J. Kim, O. Terasaki and R. Ryoo, *Chem. Mater.*, 2012, **24**, 2733-2738.
135. L.-G. Qiu, T. Xu, Z.-Q. Li, W. Wang, Y. Wu, X. Jiang, X.-Y. Tian and L.-D. Zhang, *Angew. Chem. Int. Ed.*, 2008, **47**, 9487-9491.
136. Y. Zhao, J. Zhang, B. Han, J. Song, J. Li and Q. Wang, *Angew. Chem. Int. Ed.*, 2011, **50**, 636-639.
137. W. Shang, X. Kang, H. Ning, J. Zhang, X. Zhang, Z. Wu, G. Mo, X. Xing and B. Han, *Langmuir*, 2013, **29**, 13168-13174.
138. W. Zheng, X. Hao, L. Zhao and W. Sun, *Ind. Eng. Chem. Res.*, 2017, **56**, 5899-5905.
139. B. Seoane, A. Dikhtiarenko, A. Mayoral, C. Tellez, J. Coronas, F. Kapteijn and J. Gascon, *CrystEngComm*, 2015, **17**, 1693-1700.
140. C. Avci, I. Imaz, A. Carné-Sánchez, J. A. Pariente, N. Tasios, J. Pérez-Carvajal, M. I. Alonso, A. Blanco, M. Dijkstra, C. López and D. Maspoch, *Nat. Chem.*, 2017, **10**, 78.
141. A. Carné-Sánchez, I. Imaz, M. Cano-Sarabia and D. Maspoch, *Nat. Chem.*, 2013, **5**, 203.
142. J. Sanchez-Lainez, B. Zornoza, A. Mayoral, A. Berenguer-Murcia, D. Cazorla-Amoros, C. Tellez and J. Coronas, *J. Mater. Chem. A*, 2015, **3**, 6549-6556.
143. S. Castarlenas, C. Téllez and J. Coronas, *J. Membr. Sci.*, 2017, **526**, 205-211.
144. T. Rodenas, I. Luz, G. Prieto, B. Seoane, H. Miro, A. Corma, F. Kapteijn, F. X. Llabrés i Xamena and J. Gascon, *Nature Materials*, 2014, **14**, 48.
145. B. Garai, A. Mallick, A. Das, R. Mukherjee and R. Banerjee, *Chem. Eur. J.*, 2017, **23**, 7361-7366.
146. A. Pichon, A. Lazuen-Garay and S. L. James, *CrystEngComm*, 2006, **8**, 211-214.
147. T. Friscic, *J. Mater. Chem.*, 2010, **20**, 7599-7605.
148. L. Trobs and F. Emmerling, *Faraday Discuss.*, 2014, **170**, 109-119.
149. D. Witters, N. Vergauwe, R. Ameloot, S. Vermeir, D. De Vos, R. Puers, B. Sels and J. Lammertyn, *Adv. Mater.*, 2012, **24**, 1316-1320.
150. M. Faustini, J. Kim, G.-Y. Jeong, J. Y. Kim, H. R. Moon, W.-S. Ahn and D.-P. Kim, *J. Am. Chem. Soc.*, 2013, **135**, 14619-14626.
151. G.-Y. Jeong, R. Ricco, K. Liang, J. Ludwig, J.-O. Kim, P. Falcaro and D.-P. Kim, *Chem. Mater.*, 2015, **27**, 7903-7909.
152. J. Ren, X. Dyosiba, N. M. Musyoka, H. W. Langmi, M. Mathe and S. Liao, *Coord. Chem. Rev.*, 2017, **352**, 187-219.
153. L. Paseta, B. Seoane, D. Julve, V. Sebastián, C. Téllez and J. Coronas, *ACS Appl. Mater. Interfaces*, 2013, **5**, 9405-9410.
154. S. R. Jambovane, S. K. Nune, R. T. Kelly, B. P. McGrail, Z. Wang, M. I. Nandasiri, S. Katipamula, C. Trader and H. T. Schaef, *Sci. Rep.*, 2016, **6**, 36657.
155. M. B. Majewski, A. J. Howarth, P. Li, M. R. Wasielewski, J. T. Hupp and O. K. Farha, *CrystEngComm*, 2017, **19**, 4082-4091.
156. X. Lian, Y. Fang, E. Joseph, Q. Wang, J. Li, S. Banerjee, C. Lollar, X. Wang and H.-C. Zhou, *Chem. Soc. Rev.*, 2017, **46**, 3386-3401.
157. A. Herbst, A. Khutia and C. Janiak, *Inorg. Chem.*, 2014, **53**, 7319-7333.
158. J. Della Rocca, D. Liu and W. Lin, *Acc. Chem. Res.*, 2011, **44**, 957-968.
159. W. J. Rieter, K. M. L. Taylor, H. An, W. Lin and W. Lin, *J. Am. Chem. Soc.*, 2006, **128**, 9024-9025.
160. W. J. Rieter, K. M. L. Taylor and W. Lin, *J. Am. Chem. Soc.*, 2007, **129**, 9852-9853.
161. H. Xu, X. Rao, J. Gao, J. Yu, Z. Wang, Z. Dou, Y. Cui, Y. Yang, B. Chen and G. Qian, *Chem. Commun.*, 2012, **48**, 7377-7379.
162. C. He, D. Liu and W. Lin, *Chem. Rev.*, 2015, **115**, 11079-11108.
163. T. Baati, L. Njim, F. Neffati, A. Kerkeni, M. Bouttemi, R. Gref, M. F. Najjar, A. Zakhama, P. Couvreur, C. Serre and P. Horcajada, *Chem. Sci.*, 2013, **4**, 1597-1607.
164. D. Buzek, J. Zelenka, P. Ulbrich, T. Ruml, I. Krizova, J. Lang, P. Kubat, J. Demel, K. Kirakci and K. Lang, *J. Mater. Chem. B*, 2017, **5**, 1815-1821.

TOC

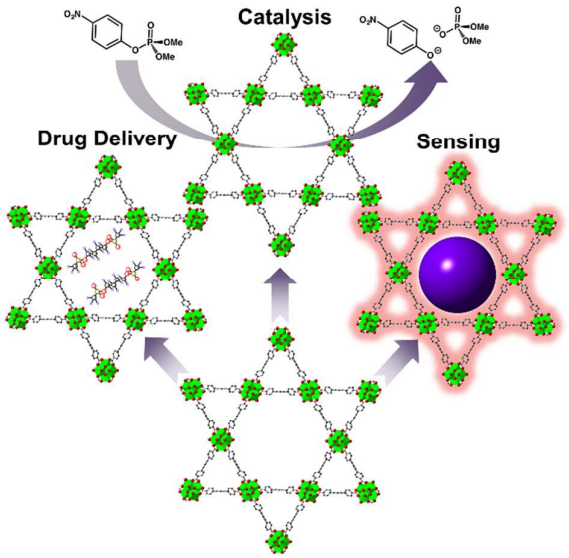

Synthetic methods for the preparation of metal–organic framework crystallites in the nano-size regime and their potentials applications are reviewed.